

# Targeting adenosine enhances immunotherapy in MSS colorectal cancer with EGFRvIII mutation

Fei Sun,<sup>1</sup> Fangzhen Yao,<sup>1</sup> Chunting Zeng,<sup>1</sup> Yang Zhao,<sup>2</sup> Bishan Liang,<sup>1</sup> Shaowei Li,<sup>1</sup> Yawen Wang,<sup>1</sup> Qijing Wu,<sup>1</sup> Yulu Shi,<sup>1</sup> Zhiqi Yao,<sup>1</sup> Jiao Wang,<sup>1</sup> Yu Jiang <sup>1</sup>, Chunhui Gu,<sup>1</sup> Qiong Huang,<sup>1</sup> Wangjun Liao <sup>1</sup>, Na Huang,<sup>1</sup> Chunlin Wang,<sup>1</sup> Xiaoxiang Rong,<sup>1</sup> Jing Wu,<sup>3</sup> Yujing Tan,<sup>4</sup> Jianjun Peng,<sup>5</sup> Yong Li,<sup>6</sup> Min Shi <sup>1</sup>

**To cite:** Sun F, Yao F, Zeng C, *et al.* Targeting adenosine enhances immunotherapy in MSS colorectal cancer with EGFRvIII mutation. *Journal for ImmunoTherapy of Cancer* 2025;**13**:e010126. doi:10.1136/jitc-2024-010126

► Additional supplemental material is published online only. To view, please visit the journal online (<https://doi.org/10.1136/jitc-2024-010126>).

FS, FY, CZ and YZ are joint first authors.

Accepted 07 January 2025

## ABSTRACT

**Background** Patients with microsatellite stable (MSS) colorectal cancer (CRC) often display resistance to immunotherapy. Epidermal growth factor receptor (EGFR)-targeted therapies have shown potential in enhancing immunotherapy, yet clinical benefits remain unfulfilled, which may relate to inadequate patient stratification.

**Methods** Circulating tumor cells and tumor tissues were collected from multicenter cohorts of patients with CRC receiving cetuximab to analyze EGFR variant type III (EGFRvIII) expression and immune infiltration. Syngeneic mouse models of EGFRvIII CRC were used to investigate the combined efficacy of adenosine inhibition and antiprogrammed cell death protein 1 (anti-PD-1).

**Results** EGFRvIII mutations are found in about 10% of MSS CRC and are associated with poor response to cetuximab therapy. EGFRvIII-mutated patients with CRC exhibit an adenosine-mediated immunosuppressive tumor microenvironment (TME) subtype. Combination therapy with adenosine inhibitors remodels the TME, reversing cetuximab resistance and enhancing anti-PD-1 efficacy in EGFRvIII CRC.

**Conclusions** Our findings identified EGFRvIII-positive CRC as a distinct subtype characterized by adenosine-mediated immunosuppressive TME. Targeting adenosine significantly improved the efficacy of anti-PD-1 in MSS CRC.

## GRAPHICAL ABSTRACT

These findings reveal a special subtype of microsatellite stable (MSS) colorectal cancer (CRC) carrying epidermal growth factor receptor variant type III (EGFRvIII) mutation, which exhibits resistance to cetuximab and immunotherapy due to impaired immune response mediated by tumor-derived adenosine. Targeting adenosine enhances antiprogrammed cell death protein 1 (PD-1) in MSS CRC, a population usually considered to be intrinsically resistant to immunotherapy. This study identifies EGFRvIII as a potential biomarker for patient stratification and individualised combined treatment. The graphical abstract was created with biorender.com.

## WHAT IS ALREADY KNOWN ON THIS TOPIC

- ⇒ Epidermal growth factor receptor variant type III (EGFRvIII) has been mainly studied in glioblastomas.
- ⇒ In colorectal cancer (CRC), the incidence of EGFRvIII and its predictive value for the efficacy of EGFR-targeted therapy such as cetuximab remain unknown.
- ⇒ Cetuximab stands out from conventional anticancer agents partly because of its potential to regulate antitumor immune response; however, few studies have explored the role of the immune microenvironment in inducing cetuximab resistance.

## WHAT THIS STUDY ADDS

- ⇒ Based on multicenter cohorts, this study shows that CRC carrying EGFRvIII mutation exhibits significant resistance to cetuximab, which is attributed to an impaired T-cell immune response mediated by tumor-derived adenosine.
- ⇒ The combined treatment of inhibitors targeting the adenosine pathway can effectively reverse cetuximab resistance and promote the efficacy of immune therapy in EGFRvIII CRC.

## HOW THIS STUDY MIGHT AFFECT RESEARCH, PRACTICE OR POLICY

- ⇒ Our findings shed light on the potential of EGFRvIII mutation as a novel biomarker, which identifies a distinct CRC phenotype characterized by cetuximab resistance and a reversible immunosuppressive environment.
- ⇒ This may pave the way for the development of immunotherapy as a feasible approach for EGFRvIII MSS CRC.

## INTRODUCTION

Immunotherapy targeting programmed cell death protein 1 (PD-1)/programmed death-ligand 1 (PD-L1) has revolutionized the treatment of malignancies<sup>1</sup>; however, immunotherapy for colorectal cancer (CRC) is challenging due to the inherent resistance to immune checkpoint inhibitor (ICI) monotherapy observed in almost 95% of patients



© Author(s) (or their employer(s)) 2025. Re-use permitted under CC BY-NC. No commercial re-use. See rights and permissions. Published by BMJ Group.

For numbered affiliations see end of article.

### Correspondence to

Professor Min Shi;  
mfyshimin@163.com



with mismatch repair proficient/microsatellite stable (MSS) tumors.<sup>2</sup> Recently, there have been significant advances, primarily focused on use of various combined strategies to reconstruct the tumor microenvironment (TME), including combination treatments incorporating molecular targeted agents.<sup>3</sup>

Cetuximab (CET), an antibody targeting epidermal growth factor receptor (EGFR), has unique advantages, demonstrating efficacy in both first-line and later-line therapies for metastatic colorectal cancer (mCRC).<sup>4</sup> Different from conventional anticancer agents, which predominantly induce non-immunogenic tumor cell death, the clinical responses observed in patients treated with CET associate with its ability to regulate immune responses. Clinical data have demonstrated enhanced cytotoxic immune infiltrates in responders following CET therapy.<sup>5</sup> In addition, CET was found to increase the immunogenicity of CRC, triggering antibody-dependent cellular cytotoxicity and immunogenic cell death.<sup>6–8</sup> Despite the initial promise of this combination strategy, only modest improvements have been observed in the clinic. The AVETUX (avelumab + cetuximab + FOLFOX) trial tested a combination of targeted antibodies, chemotherapy and the PD-L1 antibody, avelumab, for treatment of MSS CRC, and attracted considerable attention; the trial finally reported a median overall survival of 32.9 months, which is in the lower range of that achieved using the current first-line EGFR antibody and FOLFOX (fluorouracil+ leucovorin+ oxaliplatin) regimen.<sup>9</sup> Subsequent translational research identified specific subpopulations that demonstrated a trend toward enhanced clinical benefit, indicating the need for biomarker-based patient stratification.<sup>10</sup>

Gene mutation-based stratification is a fundamental requirement for the application of targeted therapies, and can also assume a pivotal role in combination strategies involving immunotherapy. A prototypical example is BRAF mutation in CRC, which leads to a unique immune infiltration pattern, as well as high expression of multiple immune checkpoint molecules.<sup>11</sup> For patients with MSS, BRAF<sup>V600E</sup> mCRC, the encorafenib+CET+nivolumab regimen proved effective and well-tolerated.<sup>12</sup> Similarly, genetic alterations of EGFR in non-small cell lung cancer are associated with weak immunogenicity and a distinct non-inflamed TME phenotype.<sup>13</sup> Several studies have uncovered that the presence of activating EGFR mutations affects the infiltration and function of diverse immune cell types, including macrophages, dendritic cells, regulatory T cells, and CD8<sup>+</sup> cytotoxic T cells, implying a possible association between EGFR mutations and compromised antitumor immunity.<sup>14–15</sup> These findings indicate the potential of EGFR mutation as a biomarker for individualized combined treatment.

The EGFR protein comprises three domains, arranged from N-terminus to C-terminus, as follows: (i) an extracellular arm responsible for ligand binding and dimerization; (ii) a hydrophobic transmembrane domain; and (iii) the intracellular tyrosine kinase and C-terminal tail

domains.<sup>16</sup> EGFR variant type III (EGFRvIII) is a constitutively active EGFR mutant caused by a deletion of exons 2–7, resulting in a truncated extracellular domain.<sup>17</sup> This mutation occurs in approximately 20% of glioblastomas<sup>16</sup> and 40% of head and neck squamous cell carcinomas,<sup>18</sup> where it is exclusively expressed in tumor cells and drives their aggressive behavior.<sup>17–19</sup> Notably, CET binds to EGFRvIII and induces downstream effects distinct from canonical EGFR pathways.<sup>20–21</sup> Furthermore, EGFRvIII can exert an impact on the tumor immune microenvironment (TIME), while co-expression of EGFR and EGFRvIII promotes macrophage infiltration via upregulation of the chemokine, CCL2, in glioblastoma.<sup>22</sup> In CRC, the incidence of EGFRvIII and its predictive value for the efficacy of EGFR-targeted therapy remain uncertain, due to limited and conflicting data.<sup>23–26</sup> Thus, further investigation into the incidence and functional role of EGFRvIII in this context is warranted.

In this study, we made a significant discovery regarding the unique characteristics of the EGFRvIII mutation, which leads to a distinct phenotype characterized by a reversibly immunosuppressive environment. We found that impaired T-cell immune responses against tumors, mediated by tumor-derived adenosine (ADO), played a crucial role in EGFRvIII-dependent resistance. Importantly, we demonstrated that inhibiting the conversion of proinflammatory ATP to immunosuppressive ADO could reverse CET resistance and significantly improve the efficacy of combined anti-PD-1 strategies in MSS CRC. Together, these findings hold great promise for application in optimizing patient stratification and present potential new therapeutic opportunities for patients with EGFRvIII MSS CRC.

## METHODS

### Human samples

Five patient cohorts in total were used for various aspects of this manuscript. All human tissue samples were collected and analyzed with approved protocols in accordance with the ethical requirements and regulations of the Institutional Review Board of Nanfang Hospital. Informed consent was obtained from all participants or their legal authorized representatives prior to sample collection. In *cohort 1*, IHC analysis was performed on the paraffin-embedded samples of primary sites obtained from 79 patients with newly diagnosed and untreated CRC, sourced from multiple centers (including Zhujiang Hospital, Ganzhou City People's Hospital, the First Affiliated Hospital of Guangzhou Medical University and Peking University Shenzhen Hospital). Furthermore, we assembled a clinical cohort of 115 patients with untreated MSS CRC using peripheral blood samples from Nanfang Hospital (*cohort 2*) and performed CTC analysis. A total of 40 patients with CRC treated with CET, whose paraffin-embedded primary tumor specimens with proficient mismatch repair (pMMR) were included for further investigation as *cohort 4*, were sourced from multiple centers,

including Nanfang Hospital, Zhujiang Hospital, The First People's Hospital of Foshan, The First Affiliated Hospital of Sun Yat-sen University, and Guangdong Provincial Hospital of Chinese Medicine. IHC and IF analysis was performed on these specimens to estimate the expression of EGFRvIII, CD39, CD73, CD8, and PD-L1. *Cohort 5* consisted of 80 patients carrying mCRC with MSS status who received CET-based therapy from Nanfang Hospital. pMMR/MSS status was confirmed by immunohistochemistry for the expression of four mismatch repair proteins (MLH1, MSH2, MSH6, and PMS2). CTC detection for EGFRvIII expression was performed using peripheral blood samples obtained from all 80 patients before initiating CET treatment. The TTP (time to progression) data of 32 patients were recorded. Dynamic CTC tests were conducted on paired blood samples every four cycles during CET treatment from 25 patients in *cohort 5*.

### Patient and public involvement

Patients or the public were not involved in the design, or conduct, or reporting, or dissemination plans of our research.

### Animal studies

BALB/c mice, C57BL/6 mice, and nude mice aged 4 weeks were obtained from the Experimental Animal Center, Nanfang Hospital, Southern Medical University. The mice were maintained at 22°C–24°C temperature, 60±10% humidity, with the 12-hour light/dark cycle, in the Animal Center of Nanfang Hospital under pathogen-free conditions. Standard rodent laboratory diet and water were provided. Littermates of the same sex were randomly assigned to experimental groups. Blinding was applied during subcutaneous injection of cell lines and measurement of tumors. To prevent confounding, MC38 or CT26 cell lines were equally divided over the animals within a cage. Untreated mice were intraperitoneally injected with normal saline. For all animal experiments, the tumor size was measured every 3 days with calipers. The tumor volume was calculated using the formula: tumor volume=( $\pi$ )/6×L×W<sup>2</sup>, where L is the long axis size and W is the vertical size. Animals were excluded from the experiments only if tumors did not form or if health concerns were reported. The mice were sacrificed individually when tumors reached >2500 mm<sup>3</sup> or when tumors showed beginning ulcer formation to prevent severe discomfort of mice. Regarding statistical calculations, for comparisons among multiple groups such as tumor growth, we opted for two-way analysis of variance (ANOVA), while for pairwise comparisons such as T-cell percentage, we used Student's t-test. The calculation of p values was based on the comparison between different groups of mice within a single experiment.

Eight in vivo experiments in total were designed in this study. In experiments 1 and 2, to investigate the impact of EGFRvIII overexpression on CET efficacy, subcutaneous tumors were constructed by injecting cells with EGFRwt or EGFRvIII overexpression into the right flank of C57BL/6

(experiment 1) or nude mice (experiment 2). On day 4 after tumor implantation, the mice were randomized into two groups (control, CET) (n=4 for each group and n=16 in total). Mice were subsequently treated with CET (Merck) at a dose of 50 mg/kg or saline by intraperitoneal injection twice weekly for 3–4 weeks. At the end point, the mice were euthanized by cervical dislocation with the tumors being collected for subsequent analysis. In experiment 3, to determine the impact of ADO pathway inhibitors on TME, 1×10<sup>6</sup> MC38 cells overexpressing EGFRvIII were injected into the right flank of C57BL/6. On day 4 after tumor implantation, the mice were randomized into six groups: control, CET (50 mg/kg, intraperitoneal injection, twice a week), POM-1 (MCE, HY-103259; 5 mg/kg, intraperitoneal injection, once daily), AMP-CP (Sigma, M8386; 20 mg/kg, intravenous injection, once daily for 1 week followed by twice weekly), CET+POM-1 and CET+AMP-CP (n=6 for each group and n=36 in total). Following 3 weeks of administration, mice were euthanized and the tumors were collected for subsequent flow cytometry (n=3 for each group) or IHC (n=3 for each group) analysis. In experiment 4, to gain insights into the dynamic changes occurring in the EGFRvIII microenvironment, MC38 EGFRvIII subcutaneous tumors were established in C57BL/6 mice using the same method described above. Three days after injection, mice were randomly divided into two groups (n=9 for each group and n=18 in total) and treated with POM-1 at a dose of 5 mg/kg or saline by intraperitoneal injection once daily, separately. On days 3, 6, and 9 following administrations, the mice were euthanized to extract lymphocytes from transplanted subcutaneous tumors for flow cytometry. In experiment 5, to evaluate the efficacy of combined regimens, C57BL/6 mice carrying subcutaneous MC38 EGFRvIII tumors were divided randomly into six groups 4 days after injection: CET+IRI, POM-1, CET+IRI+POM-1, CET+IRI+anti-PD-1, or CET+IRI+POM-1+anti-PD-1 (n=4 for each group and n=24 in total). The following 3-week treatments were given: CET, 50 mg/kg, intraperitoneal injection, twice a week; IRI, 6 mg/kg, intraperitoneal injection, once a week; POM-1, 5 mg/kg, intraperitoneal injection, once daily; anti-PD-1 (BioXcell, BE0146), 12.5 mg/kg, intraperitoneal injection, twice a week. Three weeks after administration, the mice were euthanized to assess the effectiveness and toxicity of different regimens. In addition, lymphocytes infiltrating into subcutaneous tumors were isolated for flow cytometry. In experiment 6, to achieve optimal therapeutic effect of POM-1, C57BL/6 mice carrying subcutaneous MC38 EGFRvIII tumors received four-drug combination therapy (CET+IRI+POM-1+anti-PD-1) 4 days after injection (n=4 for each group and n=16 in total). The dosing regimens of CET, IRI, and anti-PD-1 were the same as described above. For POM-1, several different dosing schedules were explored: (1) 5 mg/kg daily by intraperitoneal injection for 3 weeks; (2) 7.5 mg/kg daily by intraperitoneal injection for 3 weeks; (3) pretreatment at 5 mg/kg dose daily by intraperitoneal injection for 3 days before initiating the 3-week treatment.



Experiment 7 was conducted following the same procedure as experiment 5, except that the dosing scheme of POM-1 was pretreating mice at 5 mg/kg dose daily for 3 days before initiating the combination treatment (n=5 for each group and n=30 in total). In experiment 8, to determine whether POM-1 was able to enhance immunotherapy response in EGFRvIII-positive MSS CRC,  $1 \times 10^6$  EGFRvIII CT26 cells were injected into BALB/c mice to construct subcutaneous tumors. All the mice were randomized into four groups and subsequently treated with saline, anti-PD-1, POM-1, or anti-PD-1+POM-1, respectively (n=4 for each group and n=16 in total). When the treatment completed, mice were then sacrificed for analysis.

### Cell lines

Human CRC cell lines (HCA7 and DIFI) were obtained from Shanghai Foleibao Biotechnology Development Company. The MC38 murine colon adenocarcinoma cell line was from BNCC. The CT26 murine colon carcinoma cell line was from the National Collection of Authenticated Cell Cultures. All of the above cells were regularly tested for mycoplasma contamination and identified using short tandem repeat sequencing.

### Statistical analysis

Each experiment was repeated at least three times. Statistical analyses were performed using GraphPad Prism V.7.0 software (RRID:SCR\_002798) or SPSS V.20.0 software (RRID:SCR\_002865). For comparisons, two-way ANOVA was used for tumor growth curves and MTT assay (3-(4,5-dimethylthiazol-2-yl)-2,5-diphenyltetrazolium bromide assay). Differences between experimental groups were assessed using Student's t test, Wilcoxon test or one-way ANOVA where appropriate. Specific comparisons and analyses are described in the individual figure legends or method sections. Categorical variables are expressed as number and percentages, and continuous variables are presented as means±SD. Statistical significance was noted as a p value of <0.05.

## RESULTS

### EGFRvIII mutation is associated with poor prognosis and an immunosuppressive TME

Extensive evidence suggests that EGFR signaling contributes to the malignant progression of CRC; however, detailed clinical data regarding the prevalence and impact of EGFRvIII in CRC are lacking. Therefore, we first conducted immunohistochemical (IHC) analysis of samples from 79 patients with newly diagnosed, untreated CRC, sourced from multiple centers (*cohort 1*). In this cohort, approximately 10% (8/79) of patients tested positive for EGFRvIII (online supplemental figure S1A). Notably, EGFRvIII expression was exclusively localized to the cytoplasm and plasma membrane of tumor cells, with no expression detectable in the peri-tumoral stroma or normal mucosa. These findings are consistent

with previous reports identifying EGFRvIII as a tumor biomarker.<sup>20</sup>

To achieve more direct and precise detection of membrane-localized EGFRvIII, we next analyzed circulating tumor cells (CTCs) from peripheral blood samples of 115 patients with untreated MSS CRC by RNA fluorescence in situ hybridization using a probe specific for EGFRvIII (*cohort 2*). Strong EGFRvIII fluorescence signals originating from tumor cell membranes were observed in 12% of patients (14/115). The clinicopathological characteristics of patients with EGFRvIII-positive CRC are summarized in *cohort 2*. High EGFRvIII expression was significantly associated with tumor differentiation, lymph node metastasis, and distant metastasis (*table 1*). No significant differences in sex, age, tumor site, or clinical stage were detected between the two groups. Moreover, survival analysis performed using The Cancer Genome Atlas (TCGA) CRC cohort data (*cohort 3*; n=192) revealed markedly worse prognosis in patients with EGFRvIII-positive CRC than that in patients with EGFRvIII-negative CRC (p=0.011) (*figure 1A*). These data indicate a significant impact of EGFRvIII mutation on metastasis and patient prognosis.

To gain further insights into the association between EGFRvIII mutation and antitumor immunity, we conducted TME profiling in CRC samples using *cohort 3* data (n=192) via gene set variation analysis-based immune infiltration scoring.<sup>27</sup> The TME phenotypes of all 192 CRC samples were classified into three distinct clusters (*figure 1B*). Remarkably, the TME of EGFRvIII-positive CRC predominantly fell within cluster 1, which was characterized as an 'immune-desert' cluster, with relatively low levels of immune infiltration. Conversely, EGFRvIII-positive CRC samples were not detected in cluster 2, an immune-inflamed cluster characterized by high levels of innate and adaptive immune cell infiltration. Furthermore, EGFRvIII-positive CRC samples had significantly lower immune scores, accompanied by less T-cell infiltration, determined according to the method reported by Xiao *et al* (*figure 1C*, online supplemental figure S1B).<sup>27</sup> In addition, the expression of T-cell markers and cytokines/chemokines associated with inflammation initiation were notably reduced in EGFRvIII-positive CRC (online supplemental figure S1C).<sup>28</sup>

To investigate spatial associations between EGFRvIII and CD8<sup>+</sup> T cells in the TME, we conducted immunofluorescence (IF) analysis of tumor tissues obtained from 29 patients in *cohort 4*, comprising individuals with CET-treated MSS CRC from multiple centers. We observed markedly decreased T-cell infiltration in the TME of EGFRvIII-expressing tumors (*figure 1D*). Consistent with these clinical observations, IHC analysis of tumors in MC38 syngeneic mice also demonstrated decreased T-cell infiltration in EGFRvIII tumors relative to control tumors (*figure 1E*). Moreover, flow cytometry analysis revealed that, in addition to a reduced proportion of CD8<sup>+</sup> T cells, the production of effector cytokines by infiltrating T cells was also inhibited in EGFRvIII tumors (*figure 1F,G*).

**Table 1** Correlation between EGFRvIII mutation and clinicopathological parameters in cohort 2

	EGFRvIII negative (n=101)	EGFRvIII positive (n=14)	P value
Age (years)	60.0±14.0	61.6±10.6	0.339
Gender			0.426
Male	61 (60.4%)	10 (71.4%)	
Female	40 (39.6%)	4 (28.6%)	
Primary tumor location			0.733
Left-sided	80 (79.2%)	12 (85.7%)	
Right-sided	21 (20.8%)	2 (14.3%)	
Tumor differentiation			0.010**
Well	23 (22.8%)	0 (0%)	
Moderate	74 (73.3%)	11 (78.6%)	
Poor	4 (0.04%)	3 (21.4%)	
Undifferentiated	0 (0%)	0 (0%)	
pT stage			0.694
Tis+T1+T2	17 (16.8%)	1 (7.1%)	
T3+T4	84 (83.2%)	13 (92.9%)	
Node-positive primary			0.021*
N0	18 (17.8%)	4 (28.6%)	
N1	42 (41.6%)	6 (42.9%)	
N2	40 (39.6%)	2 (14.3%)	
N3	1 (1.0%)	2 (14.3%)	
Metastasis			0.013*
M0	72 (71.3%)	5 (35.7%)	
M1	29 (28.7%)	9 (64.3%)	
CRC stage			0.167
I	4 (4.0%)	0 (0%)	
II	13 (12.8%)	5 (35.7%)	
III	49 (48.5%)	4 (28.6%)	
IV	35 (34.7%)	5 (35.7%)	

\*P<0.05; \*\*P<0.01 (P<0.05 was considered to be significantly different).

CRC, colorectal cancer; EGFRvIII, epidermal growth factor receptor variant type III.

Collectively, these results indicate that T-cell infiltration and function are suppressed in EGFRvIII-positive CRC.

Next, we visualized the interactions between tumor-infiltrating lymphocytes (TILs) and tumor cells in the DIFI (MSS-CRC) and HCA7 (microsatellite instability-high (MSI-H)-CRC) cell lines, which are wild-type for KRAS and BRAF. We ectopically expressed EGFRvIII or wild-type EGFR (EGFRwt) in these cell lines,<sup>18</sup> and isolated CD8<sup>+</sup> T cells from healthy donor peripheral blood samples, which were then co-cultured with tumor spheroids formed by EGFRwt or EGFRvIII cells. After 48 hours co-culture, we observed declined numbers of CD8<sup>+</sup> T cells infiltrating EGFRvIII spheroids, accompanied by decreased T-cell activity (figure 1H,I, online supplemental figure S1D). Together, these data strongly imply that EGFRvIII mutation is associated with impaired antitumor immunity.

### EGFRvIII mutation facilitates CET resistance in MSS CRC

To investigate the role of EGFRvIII mutation in the unsatisfactory response of MSS CRC to combined treatment with CET and immunotherapy, we examined EGFRvIII expression in CTC samples from 80 cases of MSS mCRC collected before initiation of CET-based therapy (cohort 5). Representative images from one of these patients, showing CTCs with distinct EGFRvIII expression, are presented in figure 2A. For quantitative evaluation, an EGFRvIII scoring system was established, based on probe signal intensity and the proportion of EGFRvIII-positive CTCs. The results revealed a significant association between EGFRvIII mutation status at baseline and treatment outcome. The proportion of patients achieving at least partial response (PR) by first disease assessment in the EGFRvIII-positive group (EGFRvIII score >6) was

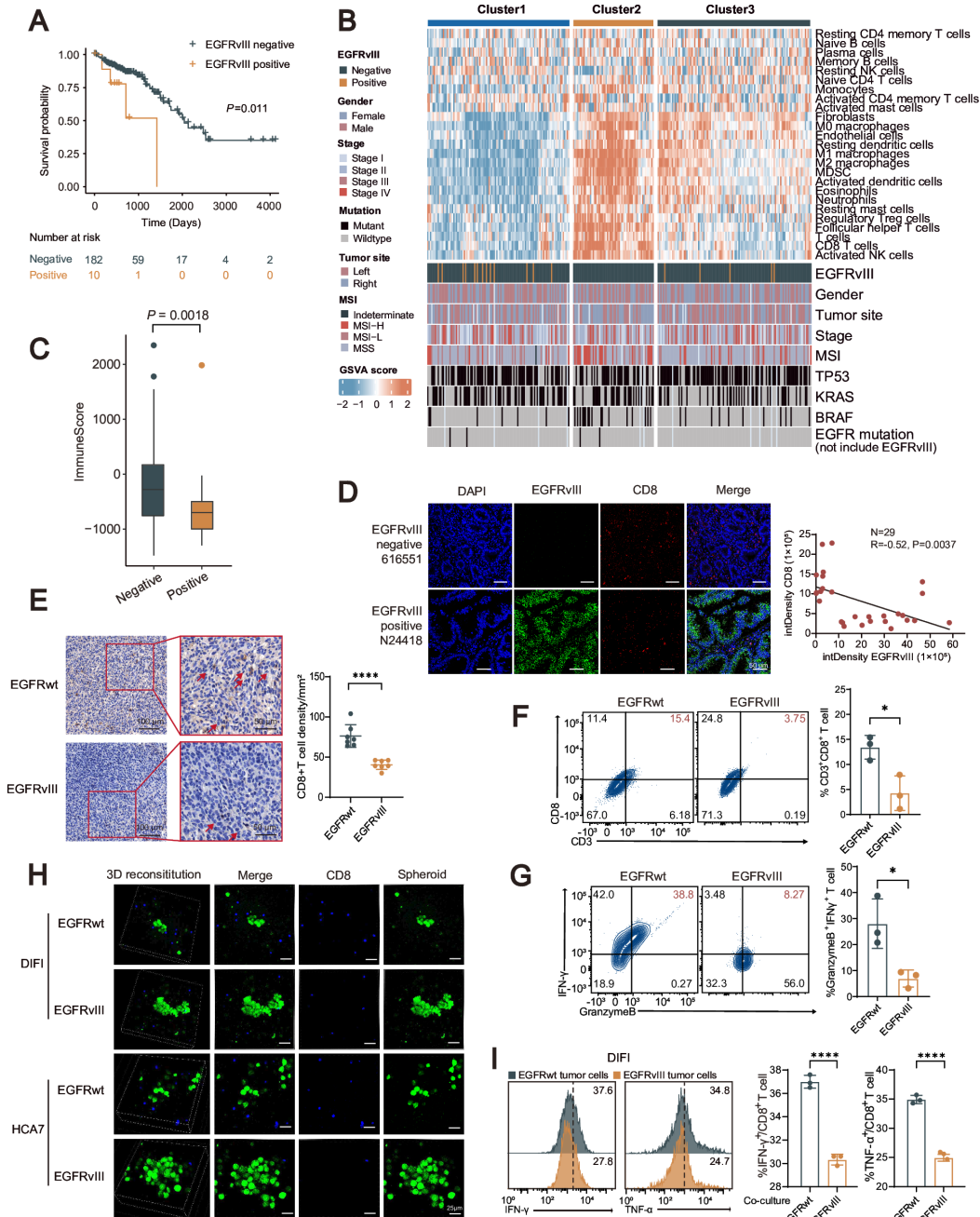


**Figure 1** EGFRvIII mutation is associated with poor prognosis and an immunosuppressive TME. (A) Kaplan-Meier OS analysis using TCGA data showing that prognosis is markedly inferior in patients with EGFRvIII-positive CRC (cohort 2,  $n=192$ ,  $p=0.011$ , log-rank test). (B) K-means clustering of CRC microenvironment phenotypes based on estimated numbers of 25 cell subsets conducted using TCGA CRC data ( $n=192$ ) and calculated by ssGSEA. (C) Immune scores of EGFRvIII-negative and EGFRvIII-positive groups in TCGA CRC cohort data ( $n=192$ ) calculated using the estimate package in R;  $p$  values were calculated using the Wilcoxon test. (D) Representative IF images of EGFRvIII and CD8 in human CRC specimens from cohort 4 (left panel) and correlation analysis of fluorescence intensity in tumor regions (right panel) ( $n=29$ ). Scale bars=50  $\mu\text{m}$ . (E) Representative IHC images showing differential CD8<sup>+</sup> T-cell infiltration in EGFRwt or EGFRvIII subcutaneous tumors in C57BL/6 mice (left panel) and quantification of CD8<sup>+</sup> T-cell density (right panel) ( $n=7$ ). (F) Lymphocytes isolated from subcutaneous tumors from each group of C57BL/6 mice were analyzed for CD3 and CD8 expression by flow cytometry (left panel), and the percentage of CD3<sup>+</sup>CD8<sup>+</sup> T cells summarized (right panel). (G) Expression of IFN- $\gamma$  and granzyme B in CD3<sup>+</sup>CD8<sup>+</sup> T cells detected using flow cytometry (left panel), and percentages of IFN- $\gamma$ <sup>+</sup> granzyme B<sup>+</sup> cells as a proportion of CD3<sup>+</sup>CD8<sup>+</sup> T cells (right panel). (H) IF staining showing CD8<sup>+</sup> T-cell infiltration into multicellular spheroids built by EGFRwt or EGFRvIII cells in a three-dimensional system. Scale bars=25  $\mu\text{m}$ . (I) Expression of IFN- $\gamma$  and TNF- $\alpha$  in isolated human CD8<sup>+</sup> T cells co-cultured with EGFRvIII DIFI cells in vitro detected by flow cytometry, along with statistical plots showing the proportions of positive cells. \* $P<0.05$ ; \*\*\*\* $P<0.0001$ . CRC, colorectal cancer; EGFRvIII, EGFR variant type III; EGFRwt, wild-type EGFR; IF, immunofluorescence; IFN, interferon; IHC, immunohistochemistry; OS, overall survival; ssGSEA, single-sample gene set enrichment analysis; TCGA, The Cancer Genome Atlas; TME, tumor microenvironment; TNF- $\alpha$ , tumor necrosis factor alfa.

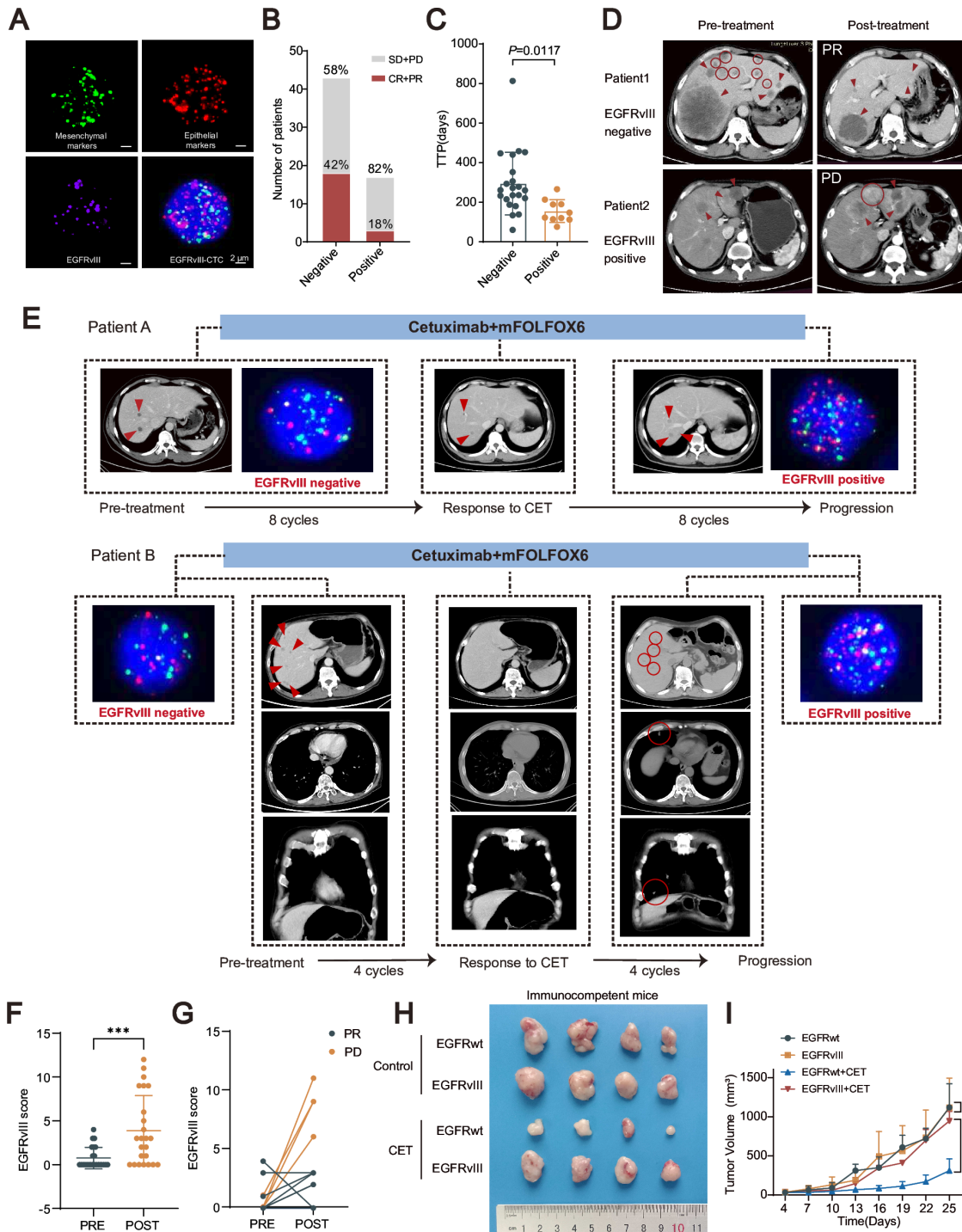


**Figure 2** EGFRvIII mutation facilitates CET resistance in MSS CRC. (A) Representative co-immunofluorescence images of CTCs from one patient with CRC expressing EGFRvIII. Tumor cells were captured using fluorescently labeled probes for epithelial biomarkers (EpCAM, CK8/18/19) or mesenchymal biomarkers (vimentin and twist). Leukocytes were excluded by CD45 staining. Scale bars=5  $\mu$ m. (B, C) The proportion of different treatment outcomes (B) and TTP (C) in groups with EGFRvIII-positive or EGFRvIII-negative CRC receiving CET-based therapy (cohort 5, n=80). (D) Longitudinal CT scans of two representative cases from the EGFRvIII-positive or EGFRvIII-negative groups showing changes in liver metastases after four cycles of CET-containing treatment. (E) Analysis of EGFRvIII expression on CTCs from two patients with CRC prior to therapy or at progression. (F, G) EGFRvIII expression levels before and after CET treatment evaluated by CTC detection in 25 patients from cohort 5. (H, I) Subcutaneous tumor model established in C57BL/6 mice using MC38 cells with EGFRwt or EGFRvIII overexpression. On day 4 after tumor implantation, mice were randomized into two groups: control and CET (n=4 per group). Representative photos of tumors on day 25 (H) and tumor growth curves on days 4–25 (I).  $P$  values were determined by two-way analysis of variance.  $^{**}P<0.01$  and  $^{***}P<0.001$ . CET, cetuximab; CR, complete response; CTC, circulating tumor cell; EGFRvIII, EGFR variant type III; EGFRwt, wild-type EGFR; MSS, microsatellite stable; ns, not significant; PD, progressive disease; PR, partial response; SD, stable disease; TTP, time to progression.

considerably lower than that in the EGFRvIII-negative group ( $0 \leq \text{EGFRvIII score} \leq 6$ ) (figure 2B). Additionally, time to progression was remarkably shorter in the EGFRvIII-positive group than that in the EGFRvIII-negative group (195 vs 294 days,  $p < 0.05$ ) (figure 2C). Representative CT images of the upper abdomen of a patient with EGFRvIII-positive CRC demonstrating liver metastasis progression after four cycles of CET-containing treatment are presented in figure 2D. Intriguingly, in two patients who were initially EGFRvIII-negative and achieved PR during the first evaluation, a newly emerged EGFRvIII mutation was detected on tumor progression during regular CTC evaluation. The clinical history of each patient is presented in figure 2E.

Furthermore, we performed CTC tests on paired blood samples collected before and after treatment from 25 patients in cohort 5. Surprisingly, increased EGFRvIII scores were detected in almost all patients following CET treatment, regardless of their clinical response; score increases were particularly pronounced in patients experiencing progressive disease (figure 2F–G). These data corroborate the relevance of EGFRvIII to CET efficacy in treatment of mCRC.

Consistent with our clinical observations, CET failed to impede the rapid growth of EGFRvIII-positive tumors relative to its remarkable therapeutic effect against EGFRwt tumors in MC38 (wild-type KRAS and BRAF) syngeneic mice (figure 2H,I). IHC analysis revealed that EGFRvIII-positive tumors exhibited higher proliferative activity and less apoptosis than EGFRvIII-negative tumors (online supplemental figure S2A). Notably, tumor models in immunodeficient nude mice showed that EGFRvIII and EGFRwt tumors grew at similar rates in both control and treatment groups (online supplemental figure S2B,C). Moreover, no significant differences in proliferation or CET sensitivity were observed between EGFRwt and EGFRvIII cells in vitro (online supplemental figure S2D–F). This phenomenon was further confirmed using three-dimensional multicellular spheroids (online supplemental figure S2G). Collectively, these observations reveal that the drug resistance of EGFRvIII CRC is attributable to impaired antitumor immune responses, rather than resistance intrinsic to the cells themselves.

### Tumor-derived ADO impairs T-cell infiltration and function in EGFRvIII-positive CRC

To determine whether the inhibition of TILs by EGFRvIII tumor cells was dependent on direct cell contact, we collected conditioned medium (CM) from CET-pretreated EGFRvIII or EGFRwt cells via ultracentrifugation. Supernatants from EGFRvIII cells more potently suppressed IFN- $\gamma$  and TNF- $\alpha$  expression in CD8<sup>+</sup> T cells than those from EGFRwt cells (figure 3A,B). In addition, in vitro killing assays confirmed that supernatants of EGFRvIII cells (figure 3C,D) impaired T-cell killing activity (online supplemental figure S3A,B). These results indicate that soluble low-molecular-weight immunosuppressive

factor(s) derived from EGFRvIII tumors mediated the T-cell function inhibition.

Subsequently, we performed depletion experiments, targeting different components in the cell supernatants. Proteinase K, which eliminates proteins, and fumed silica, which removes lipids, did not alter the immunosuppressive properties of EGFRvIII-CM (figure 3E); however, removal of small molecules from EGFRvIII-CM using dextran-coated charcoal (DCC) resulted in significant restoration of T-cell function (figure 3E). To further support this conclusion, we fractionated EGFRvIII-CM using a 3 kDa molecular-weight-cutoff filter. The fraction containing molecules  $< 3$  kDa exhibited similar immunosuppressive activity to complete EGFR-CM (figure 3F,G). These results confirm that the soluble factor(s) responsible for inhibiting T-cell function in EGFRvIII-positive CRC are small molecules, rather than proteins, lipids, or large peptides.

To elucidate the specific components mediating T-cell suppression, we used ESI-Q TRAP-MS/MS to complement the untargeted metabolite analysis of EGFRwt-CM and EGFRvIII-CM. Of the top 15 differential metabolites, ADO was markedly elevated in EGFRvIII-CM (figure 3H). ADO exerts its effects in regulating the function of various immune cells by binding to one of four ADO receptors: A1R, A2AR, A2BR, and A3R. To investigate whether ADO-mediated mechanisms are involved in EGFRvIII-induced T-cell suppression, we next detected ADO levels in cell supernatants, and found that EGFRvIII-CM contained higher concentrations of ADO than EGFRwt-CM (figure 3I). Moreover, addition of exogenous ADO remarkably increased the immunosuppressive capacity of EGFRwt-CM (figure 3J, online supplemental figure S3C). The predominant ADO receptor subtype on T cells, A2AR, is known to mediate ADO-induced inhibition of T-cell activity,<sup>29</sup> and treatment with an A2AR inhibitor, ZM241385, effectively reversed the suppression of T-cell effector cytokines production induced by EGFRvIII-CM (figure 3K). These findings suggest that EGFRvIII tumor cells evade T cell-mediated antitumor immune responses by elevating extracellular ADO concentrations.

### EGFRvIII tumor cells facilitate extracellular ATP-to-ADO transition via the CD39/CD73 pathway

ADO in the TME primarily originates from the sequential hydrolysis of ATP by the coordinated action of the cell-surface ectonucleotidases, CD39 and CD73.<sup>30</sup> Significantly higher levels of both CD39 and CD73 expression were observed in EGFRvIII cells relative to those in EGFRwt cells (figure 4A,B). Consistently, IF staining of histological sections from patients in cohort 4 demonstrated stronger CD39 and CD73 fluorescence signals in EGFRvIII-expressing samples relative to EGFRvIII-negative areas (figure 4C). These specimens exhibited a correlation between EGFRvIII and CD39/CD73 levels measured based on IF intensity (figure 4D,E). Moreover, correlation and colocalization analysis revealed co-expression of CD39 and CD73 in EGFRvIII-positive tissues

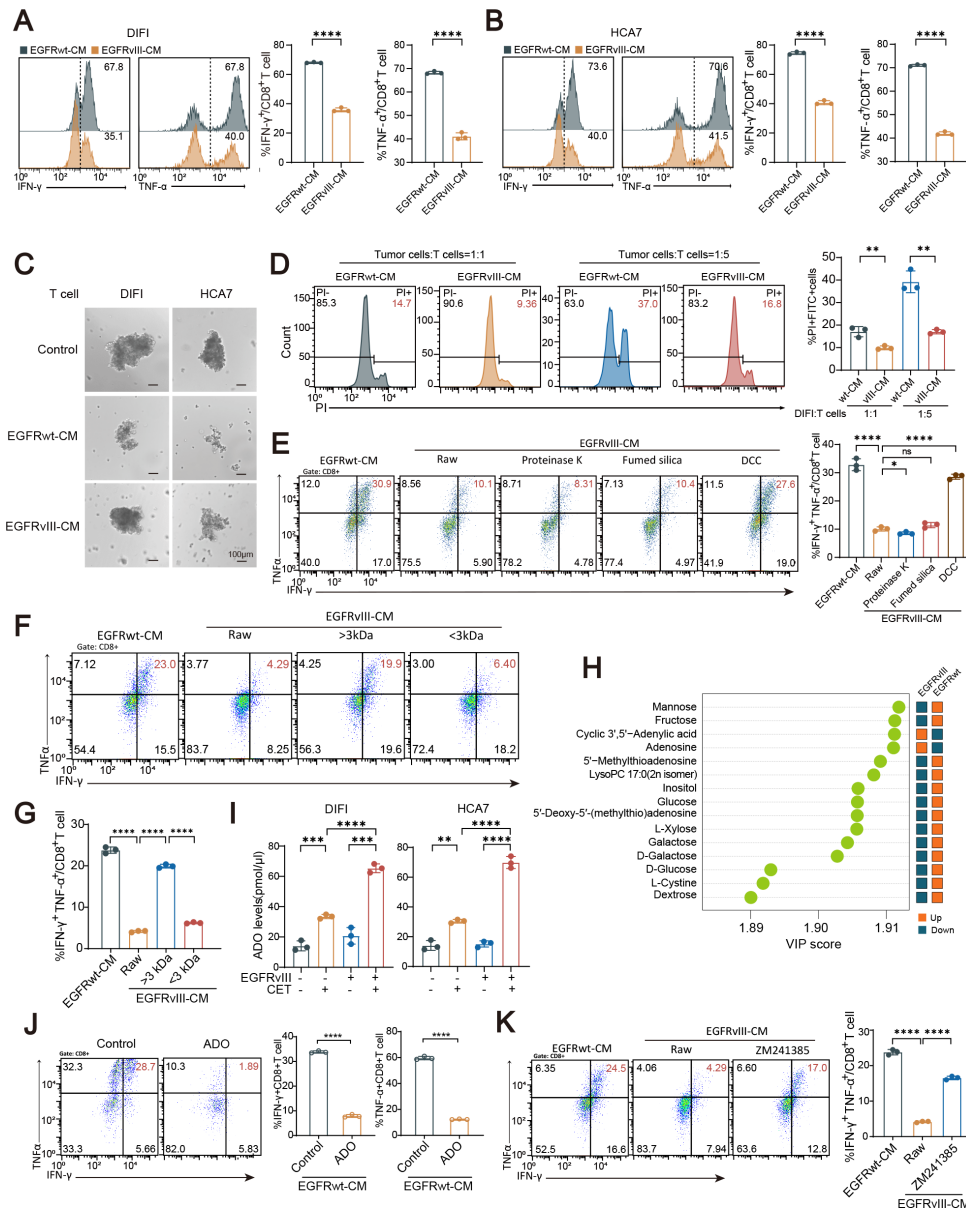


**Figure 3** Tumor-derived ADO impairs T-cell infiltration and function in EGFRvIII-positive CRC. (A–B) In vitro IFN- $\gamma$  and TNF- $\alpha$  expression in isolated human CD8<sup>+</sup> T cells treated with CM from DIFI (A) or HCA7 (B) cells detected using flow cytometry (left panels), along with statistical plots of the proportions of positive cells (right panels). (C) Representative pictures reflecting the variation of multicellular spheroids established by DIFI or HCA7 tumor cells co-cultured with EGFRwt-CM-pretreated or EGFRvIII-CM-pretreated human CD8<sup>+</sup> T cells in vitro. Scale bars=100  $\mu$ m. (D) Representative flow cytometry plots (left panels) and proportions of apoptotic tumor cells (right panel) when DIFI cells were incubated with EGFRwt-CM-pretreated or EGFRvIII-CM-pretreated human CD8<sup>+</sup> T cells at 1:1 or 1:5 ratios. (E) Expression of IFN- $\gamma$  and TNF- $\alpha$  by isolated human CD8<sup>+</sup> T cells detected by flow cytometry following exposure to CM depleted of proteins, lipids and small molecules (left panels), along with statistical plots of the proportions of positive cells (right panels). (F, G) Expression of IFN- $\gamma$  and TNF- $\alpha$  by isolated human CD8<sup>+</sup> T cells detected by flow cytometry following exposure to CM fractions <3 kDa or >3kDa (F), along with statistical plots of the proportions of positive cells (G). (H) Untargeted metabolite analysis of EGFRwt-CM and EGFRvIII-CM by ESI-Q TRAP-MS/MS. Metabolites were considered differentially regulated based on threshold values of  $p < 0.05$  and VIP (based on the OPLS-DA model)  $> 1$ . The top 15 differential metabolites are shown. (I) Adenosine levels in medium of cells with or without CET treatment determined using an Adenosine Assay Kit (Abcam). (J) Expression of IFN- $\gamma$  and TNF- $\alpha$  in isolated human CD8<sup>+</sup> T cells determined by flow cytometry following exposure to EGFRvIII-CM, with or without additional ADO (left panels), along with statistical plots of the proportions of positive cells (right panels). (K) Expression of IFN- $\gamma$  and TNF- $\alpha$  in isolated human CD8<sup>+</sup> T cells determined by flow cytometry following exposure to EGFRvIII-CM under A2AR inhibition using ZM241385 (left panels), along with statistical plots of the proportions of positive cells (right panels). Data are the mean  $\pm$  SEM values of at least three independent experiments, \* $P < 0.05$ , \*\* $P < 0.01$ , \*\*\* $P < 0.001$ , and \*\*\*\* $P < 0.0001$ . ADO, adenosine; CM, conditioned medium; CRC, colorectal cancer; DCC, dextran-coated charcoal; EGFRvIII, EGFR variant type III; EGFRwt, wild-type EGFR; IFN, interferon; ns, not significant; OPLS-DA, orthogonal projections to latent structures discriminant analysis; TNF- $\alpha$ , tumor necrosis factor alpha; VIP, variable importance in the projectio.

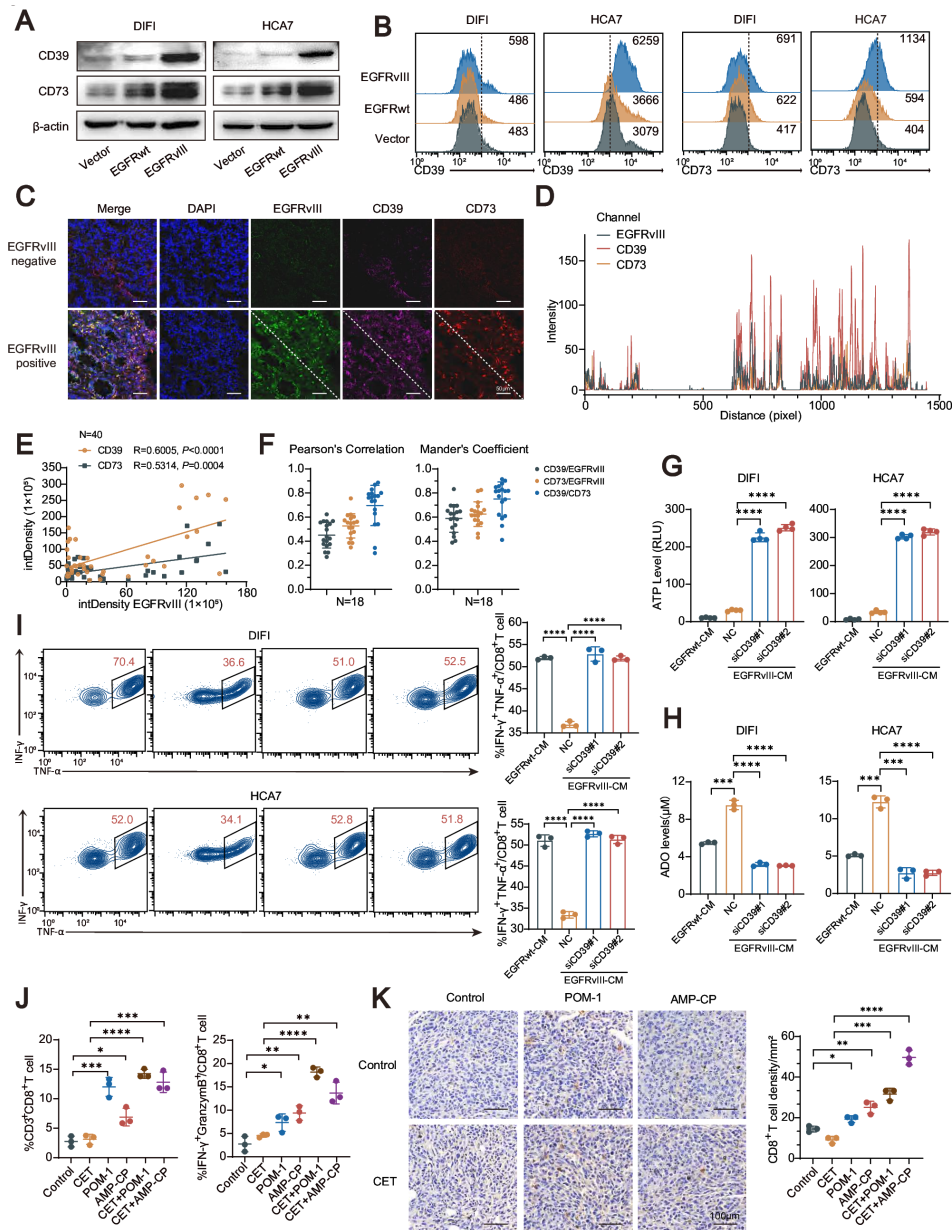


**Figure 4** EGFRvIII tumor cells facilitate extracellular ATP-to-ADO transition via the CD39/CD73 pathway. (A) CD39 and CD73 expression in vector-transfected, EGFRwt and EGFRvIII cells determined by western blot analysis. (B) Representative flow cytometry plots showing CD39 and CD73 expression on the cell membranes of vector-transfected, EGFRwt and EGFRvIII cells. (C–F) Expression of EGFRvIII, CD39, and CD73 detected by IF in human CRC specimens from cohort 4 (n=40). Representative IF images of EGFRvIII-negative and EGFRvIII-positive tissues (C) and quantification of fluorescent intensity at each position along the indicated diagonal (D). CD39 and CD73 expression were positively correlated with EGFRvIII expression in CRC (linear regression) (E). Pearson's correlation coefficient (left panel) and Mander's overlap coefficient (right panel) values were calculated to analyze the colocalization of EGFRvIII with CD39/CD73 (n=18) (F). (G) ATP levels in the medium of EGFRvIII cells after silencing CD39, determined using an ATP Assay Kit (Beyotime). (H) Adenosine levels in the medium of EGFRvIII cells after silencing CD39, determined using an Adenosine Assay Kit (Abcam). (I) Expression of IFN- $\gamma$  and TNF- $\alpha$  by isolated human CD8<sup>+</sup> T cells following exposure to CM from EGFRvIII cells with CD39 silenced, tested by flow cytometry (left panels), along with statistical plots of the proportions of positive cells (right panels). (J, K) Subcutaneous tumor model in C57BL/6 mice established using MC38 EGFRvIII cells. On day 4 after tumor implantation, mice were randomized into six groups: control, CET, POM-1, AMP-CP, CET+POM-1, and CET+AMP-CP. Following 3 weeks of treatment, lymphocytes isolated from subcutaneous tumors from each group were analyzed for CD3, CD8, IFN- $\gamma$ , and granzyme B expression by flow cytometry. Percentages of CD3<sup>+</sup>CD8<sup>+</sup> T cells (left panel) and of IFN- $\gamma$ <sup>+</sup> granzyme B<sup>+</sup> cells as a proportion of CD3<sup>+</sup>CD8<sup>+</sup> T cells are summarized (right panel) (J). CD8<sup>+</sup> T-cell infiltration into subcutaneous tumors of each group analyzed by IHC staining. Representative IHC images (left panel) and quantification of the density of CD8<sup>+</sup> T cells (right panel) (K). Scale bars=100  $\mu$ m. Data are the mean $\pm$ SEM values of at least three independent experiments. \*P<0.05, \*\*P<0.01, \*\*\*P<0.001, and \*\*\*\*P<0.0001. ADO, adenosine; CET, cetuximab; CM, conditioned medium; CRC, colorectal cancer; EGFRvIII, EGFR variant type III; EGFRwt, wild-type EGFR; IF, immunofluorescence; IFN, interferon; IFN, interferon; IHC, immunohistochemistry; TNF- $\alpha$ , tumor necrosis factor alpha.

(figure 4F). To further investigate the functional roles of CD39 and CD73 in ADO production and T-cell inhibition, we silenced CD39 expression in EGFRvIII cells and observed reduced ADO and increased ATP content in the harvested supernatants, accompanied by an attenuated capacity to inhibit T-cell cytokine secretion (figure 4G–I, online supplemental figure S4A). Similar results were obtained using the CD39 inhibitor, POM-1 and the CD73 inhibitor, AMP-CP (online supplemental figure S4B–C). Together, these data indicate that ADO production regulated by CD39 and CD73 is aberrantly active in EGFRvIII tumor cells, leading to an immunosuppressive TME.

Next, to determine whether targeting ADO production could reshape the TME *in vivo*, we treated MC38 EGFRvIII tumor-bearing mice with POM-1 or AMP-CP, either alone or in combination with CET. Combination therapy with POM-1 or AMP-CP improved both CD8<sup>+</sup> T-cell infiltration and their cytokine expression, which were inhibited in EGFRvIII tumors (figure 4J, online supplemental figure S4D). Consistently, IHC demonstrated a remarkable increase in T-cell numbers in tumors from the two combination therapy groups compared with the CET-treated group (figure 4K). Furthermore, to gain insights into the dynamic changes occurring in the EGFRvIII TME, we performed serial flow cytometry analyses. The results showed that enhanced T-cell infiltration in the POM-1 group compared with the control group was detectable as early as day 3 (online supplemental figure S4E). With prolonged POM-1 treatment, the cytotoxic activity of TILs was noticeably improved (online supplemental figure S4F). These findings collectively demonstrate that inhibiting ADO production by targeting CD39 or CD73 can effectively overcome EGFRvIII-induced T-cell suppression, thereby transforming ‘cold’ tumors into ‘hot’ ones.

### Phosphorylated STAT3 upregulates CD39/CD73 expression in EGFRvIII-positive CRC

To address the regulatory mechanism underlying CD39 and CD73 expression, we next conducted gene set enrichment analysis using TCGA CRC cohort data (cohort 3, n=192). The analysis revealed that genes highly correlated with EGFRvIII were enriched in the STAT3 pathway, indicating a potential association (online supplemental figure S5A). IF staining demonstrated a significant increase in phosphorylated STAT3 (p-STAT3) in both EGFRwt-overexpressing and EGFRvIII-overexpressing cells relative to vector-transfected cells (figure 5A). Through subsequent nuclear-cytoplasmic fractionation experiment followed by western blot (WB) analysis, we found that the expression of p-STAT3 was markedly elevated both in cytoplasm and nucleus of EGFRvIII cells, compared with EGFRwt cells (figure 5B). Following phosphorylation, STAT3 dimerizes and translocates into the nucleus, where it acts as a transcription factor to induce target gene expression.<sup>31 32</sup> In glioblastoma, EGFRvIII regulates the STAT3 pathway through multiple mechanisms,<sup>20</sup> yet there have been no reports of a direct effect of STAT3 on ADO metabolism. We hypothesized that p-STAT3 may

act as a transcription factor to regulate CD39 and CD73 expression. To test this possibility, we treated EGFRvIII cells with small interfering RNA (siRNA) targeting STAT3 or STA-21, a chemical inhibitor of STAT3 dimerization and binding to DNA.<sup>33</sup> Notably, STAT3 inhibition significantly reversed the elevated expression of CD39 and CD73 in EGFRvIII cells, as confirmed by quantitative real-time PCR (qRT-PCR), IF, and WB assays (figure 5C–F, online supplemental figure S5B–H). Moreover, inhibiting STAT3 activity impaired the conversion of ATP to ADO in EGFRvIII-CM and attenuated its inhibitory effect on T-cell cytokine secretion (figure 5G–J). Furthermore, chromatin immunoprecipitation-qRT-PCR demonstrated that STAT3 can indeed bind to the promoter regions of genes encoding both CD39 and CD73 (figure 5K,L). Together, these results indicate that STAT3 regulates CD39 and CD73 expression via binding to their promoter regions.

### Blocking ADO generation reignites the immunologically ‘cold’ TME to synergize with immunotherapy

Our results demonstrate that extracellular ADO, derived from EGFRvIII-positive CRC, inhibited T-cell infiltration and activity, leading to resistance to combined treatment with CET and immunotherapy. Interestingly, IF staining of tissue sections from patients in cohort 4 revealed a significant correlation between IF intensity of EGFRvIII and that of PD-L1 (online supplemental figure S6A,B). Consistently, WB and flow cytometry analyses showed that EGFRvIII-CM led to upregulation of PD-L1 expression in EGFRwt cells (online supplemental figure S6C); this effect was attenuated by inhibition of ADO production (online supplemental figure S6D–G). These results suggest a potential role for extracellular ADO in regulating PD-L1 expression through intercellular communication.

Based on the observations described above, we next conducted *in vivo* experiments to evaluate the efficacy of combined treatment using CET+irinotecan (IRI) with POM-1, anti-PD-1, or POM-1+anti-PD-1, for EGFRvIII tumors. CET+IRI alone was ineffective in suppressing tumor growth, indicating *in vivo* resistance (online supplemental figure S7A,B). Notably, CET+IRI+anti-PD-1 administration did not achieve satisfactory therapeutic effects (online supplemental figure S7A,B). In contrast, a triple combination regimen (CET+IRI+POM-1) remarkably stimulated CD8<sup>+</sup> T-cell infiltration in the TME, resulting in delayed tumor progression (online supplemental figure S7C–E). The four-drug combination group (CET+IRI+POM-1+anti-PD-1) exhibited the highest efficacy in improving T-cell infiltration, as demonstrated by flow cytometry analysis (online supplemental figure S7C–E). In summary, targeting ADO production in the TME has potential to improve the sensitivity of EGFRvIII-positive CRC to CET and immunotherapy, and thus represents a promising combinatorial strategy.

Disruption of the TIME is responsible for the inherent resistance of MSS CRC to immunotherapy. Thus, it is critical to abolish such immunosuppression prior to

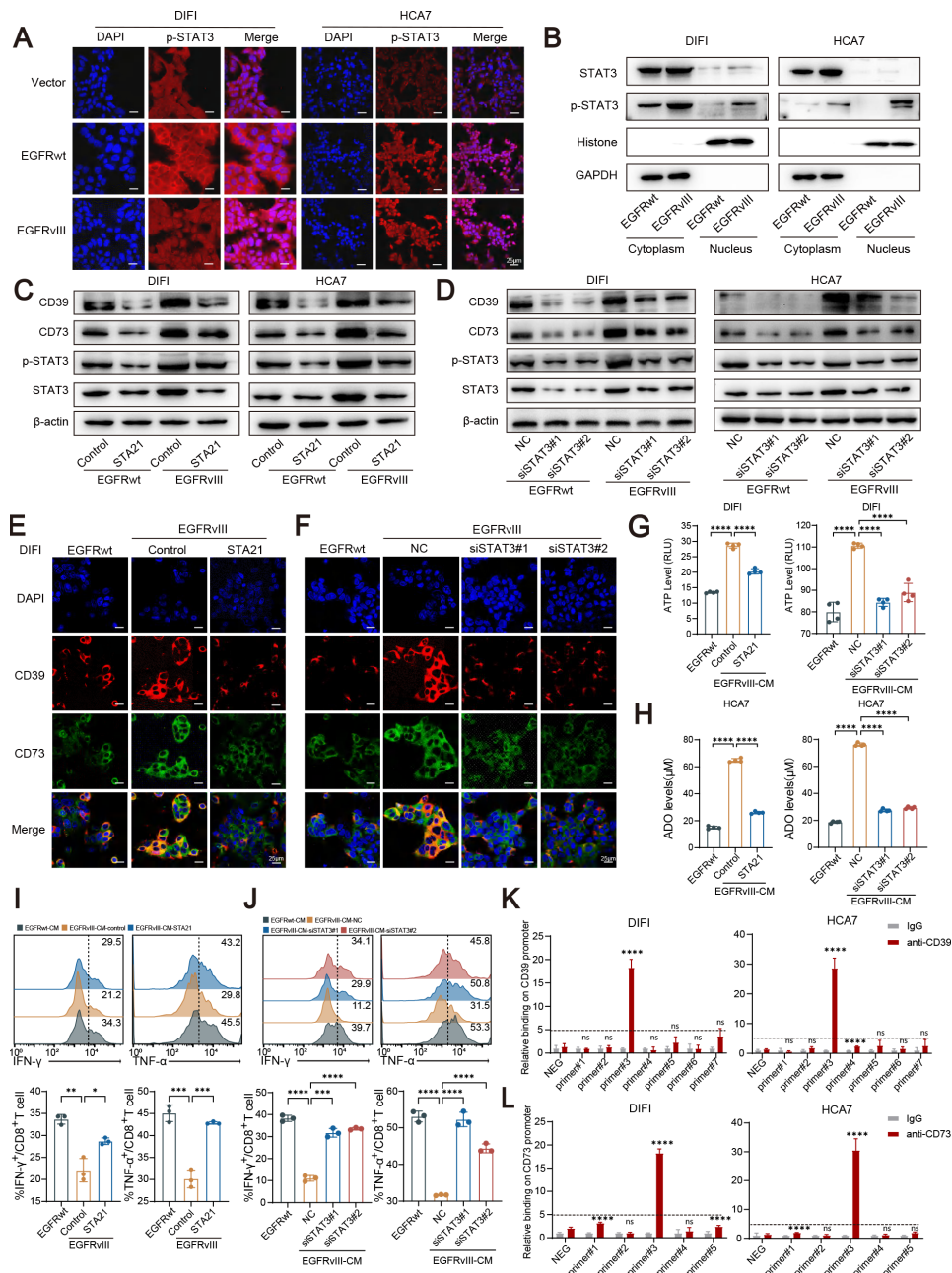


**Figure 5** p-STAT3 upregulates CD39/CD73 expression in EGFRvIII-positive CRC. (A) IF staining showing p-STAT3 was notably elevated in EGFRvIII cells compared with EGFRwt cells. Scale bars=25  $\mu$ m. (B) Intracellular distribution of p-STAT3 detected by nuclear-cytoplasmic fractionation experiment followed by western blot analysis. (C, D) CD39 and CD73 protein levels detected by western blot analysis in EGFRwt or EGFRvIII tumor cells after inhibition of STAT3 using STA-21 (C) or siRNAs (D). (E, F) Representative IF images showing CD39 and CD73 expression in DIFI EGFRvIII tumor cells after STAT3 inhibition using STA-21 (E) or siRNAs (F) detected by western blot analysis. Scale bars=25  $\mu$ m. (G) ATP levels in the culture medium of EGFRvIII cells after STAT3 inhibition using STA-21 (left panel) or siRNAs (right panel) determined using an ATP Assay Kit (Beyotime). (H) Adenosine levels in the culture medium of EGFRvIII cells after STAT3 inhibition using STA-21 (left panel) or siRNAs (right panel) determined using an Adenosine Assay Kit (Abcam). (I) Expression of IFN- $\gamma$  and TNF- $\alpha$  by isolated human CD8<sup>+</sup> T cells tested by flow cytometry following exposure to CM from EGFRvIII cells treated with STA-21 (top panels), along with statistical plots of the proportions of positive cells (bottom panels). (J) Expression of IFN- $\gamma$  and TNF- $\alpha$  in isolated human CD8<sup>+</sup> T cells tested by flow cytometry following exposure to CM from EGFRvIII with STAT3 silenced (top panels), along with statistical plots of the proportions of positive cells (bottom panels). (K, L) EGFRvIII cells were harvested for ChIP assay to detect p-STAT3 enrichment around the promoters of genes encoding CD39 (K) and CD73 (L). Immunoprecipitated DNA was analyzed by qRT-PCR using specific primers. Anti-IgG antibody served as the negative control. Data are presented as mean $\pm$ SEM values of at least three independent experiments. \* $P$ <0.05, \*\* $P$ <0.01, \*\*\* $P$ <0.001, and \*\*\*\* $P$ <0.0001. ChIP, chromatin immunoprecipitation; CM, conditioned medium; CRC, colorectal cancer; EGFRvIII, EGFR variant type III; EGFRwt, wild-type EGFR; IF, immunofluorescence; IFN, interferon; p-STAT3, phosphorylated STAT3; qRT-PCR: quantitative real-time PCR; siRNA, small interfering RNA; TNF- $\alpha$ , tumor necrosis factor alfa.

administration of anti-PD-1/PD-L1 therapy. In the *in vivo* experiment described above, we established a basal dosing regimen for POM-1, administering 5 mg/kg daily via intraperitoneal injection for 3 weeks, following previous reports.<sup>34,35</sup> To further improve the therapeutic effect of the four-drug combination therapy, we tested two optimized regimens, as follows: (1) escalating POM-1 dose to 7.5 mg/kg daily for 3 weeks and (2) pretreating mice with POM-1 at 5 mg/kg daily for 3 days, before initiating the combination treatment. Compared with the basal regimen, the 7.5 mg/kg POM-1 daily dosing regimen further promoted CD8<sup>+</sup> T-cell infiltration and activity, resulting in improved antitumor effects (figure 6A,B). Furthermore, despite the relatively minor adjustment in the total POM-1 dosage, the pretreatment scheme achieved almost identical outcomes to the 7.5 mg/kg dosing regimen (figure 6C–E). Considering the dynamic changes observed in the TME following POM-1 treatment, it is plausible that POM-1-induced TIME remodeling created a favorable ‘soil’ for the immune-activating effects of CET and anti-PD-1; therefore, we repeated the *in vivo* experiment, to compare different therapeutic strategies based on the POM-1 pretreatment scheme. Remarkably, advance POM-1 administration led to a more prominent reduction in EGFRvIII tumor size in both the triple (CET+IRI+POM-1) and four-drug (CET+IRI+POM-1+anti-PD-1) combination groups (figure 6F,G). Flow cytometry analysis also revealed a distinct elevation in the TIL population and their secretion of cytotoxic cytokines (figure 6H–J).

We next investigated whether targeting ADO metabolism could overcome anti-PD1 resistance in MSS CRC using a syngeneic CT26 (MSS CRC) tumor model. CT26 cells overexpressing EGFRvIII were injected into the syngeneic mice and the resulting tumors subsequently treated with saline, anti-PD-1, POM-1, or anti-PD-1+POM-1. Relative to anti-PD-1 or POM-1 monotherapy, we found that the combination of both drugs significantly inhibited tumor growth, with no apparent toxicity (figure 6K,L). Combination therapy exerted promising effects in reducing ADO concentration, facilitating T-cell infiltration, and increasing the proportion of IFN- $\gamma$ <sup>+</sup> or TNF- $\alpha$ <sup>+</sup> TILs (figure 6M, online supplemental figure S7F–G). These findings suggest that a small molecular inhibitor of CD39 has potential as a potent enhancer of immunotherapeutic agents in the EGFRvIII-positive subgroup, while also highlighting the potential of EGFRvIII as a novel biomarker for the application of immunotherapy in MSS CRC.

## DISCUSSION

Recent studies have highlighted the profound impact of EGFR inhibition on TME plasticity, suggesting its influence in driving drug resistance.<sup>36</sup> Here, we discovered that EGFRvIII-positive CRC shaped an immunosuppressive TME mediated by ADO, thereby leading to a decline in efficacy of strategies combining CET with immunotherapy. By inhibiting CD39, we observed an

improvement in immune cell infiltration and a reversal of drug resistance. This breakthrough paves the way for immunotherapy development as a feasible approach for EGFRvIII-positive MSS CRC.

CET has demonstrated efficacy in both first-line and later-line therapies for mCRC<sup>4</sup>; however, the frequent occurrence of resistance severely limits its therapeutic benefits. Previous investigations of CET resistance have primarily focused on genetic alterations within the downstream signaling cascade and abnormal activation of parallel bypass pathways,<sup>37</sup> neglecting the ability of CET to regulate antitumor immune responses. Interestingly, a recent study revealed an absence of known CET resistance driver gene aberrations in up to 64% of biopsy samples from patients experiencing disease progression,<sup>5</sup> highlighting the potential influence of non-genetic factors on CET resistance. Furthermore, another study observed significantly enhanced cytotoxic immune infiltrates in responders following CET therapy.<sup>5</sup> An interim analysis of the AVETUXIRI trial conducted in 2021 showed that the clinical efficacy of a combined regimen, comprising anti-PD-L1 avelumab with CET and IRI, for MSS CRC largely depended on adaptive immune response activation.<sup>38</sup> Thus, accumulating evidence underscores the crucial role of the TIME in effective CET treatment, whether CET is the central component in conventional combined chemotherapy regimens, or has a supporting function in combination immunotherapies; however, the mechanisms underlying CET resistance-associated TIME remodeling remain largely unknown.

In this research, we found that EGFRvIII-related resistance to CET can be attributed to an impaired T-cell immune response, which is mediated by tumor-derived ADO. In addition, PD-L1 upregulation was observed in EGFRwt cell membranes following treatment with EGFRvIII-CM; this finding was further validated by the observed correlation between EGFRvIII and PD-L1 expression in clinical specimens and suggests an additional mechanism, whereby EGFRvIII reshapes immune responses by specifically promoting PD-L1 expression on neighboring EGFRwt cells through paracrine signaling, contributing to an overall immune escape strategy. These phenomena provide compelling evidence of the intricate interplay between genetic factors, such as EGFR mutations, and non-genetic factors, such as the immune microenvironment, in the development of resistance, providing a new perspective for future investigations into CET resistance mechanisms.

ADO is an important molecule in TME metabolic and immune interactions, and ADO-related metabolic pathways are active in various tumors.<sup>29</sup> Multiple inhibitors or monoclonal antibodies targeting CD39 and CD73 have entered clinical trials to explore a comprehensive strategy targeting ADO metabolism combined with ICIs.<sup>39,40</sup> Our findings identified ADO as an important mediator of the interaction between EGFRvIII mutation and the immune microenvironment in both MSS and MSI-H CRC, laying the foundation for potential combination therapy. We

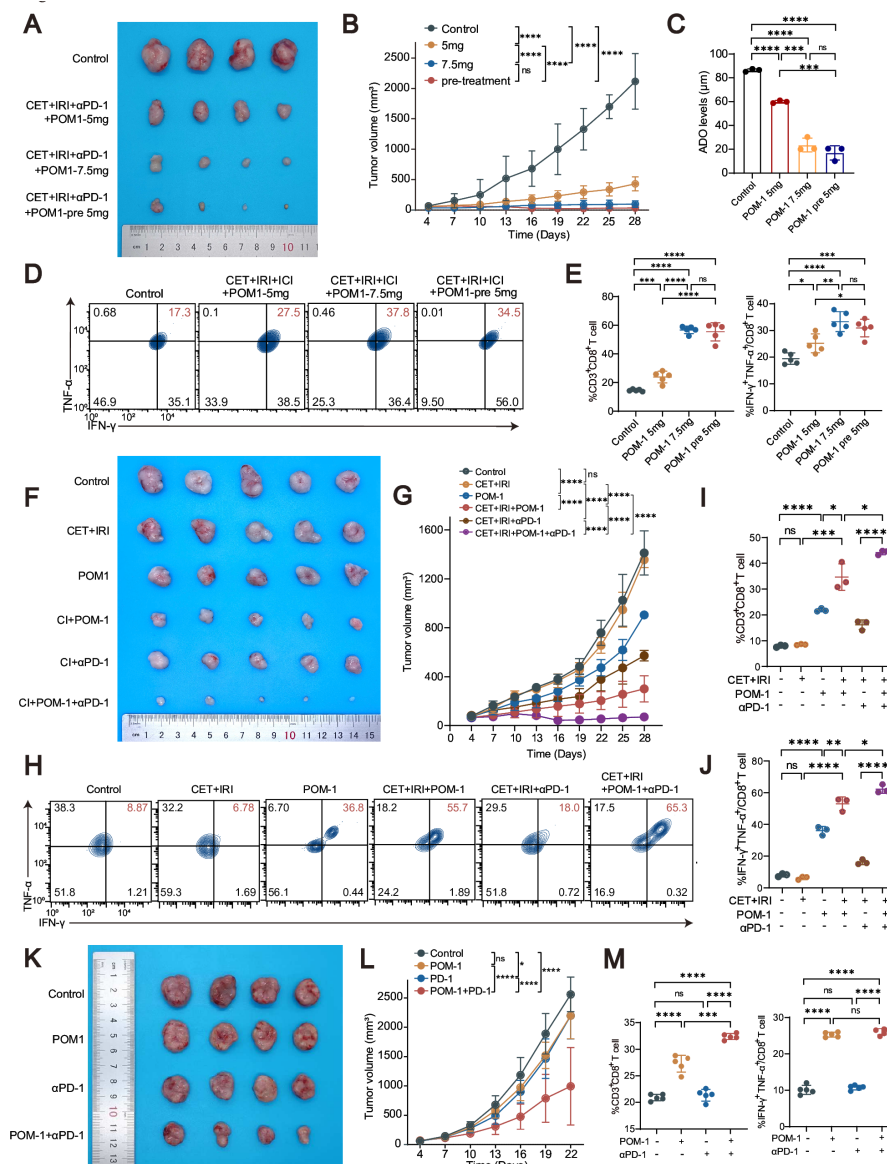


**Figure 6** Blocking ADO generation reignites the established immunologically 'cold' TME to synergize with immunotherapy. (A–E) C57BL/6 mice carrying subcutaneous MC38 EGFRvIII tumors received four-drug combination therapy, including POM-1 administered using different dosing schemes ( $n=4$  per group). Representative images of subcutaneous tumors from each group harvested on day 28 (A). Tumor growth curves on day 4–28 postinjection with MC38 EGFRvIII cells. Tumor volumes were calculated every 3 days (B). P values were determined by two-way ANOVA. ADO levels in the supernatants of subcutaneous tumor tissues were detected using an Adenosine Assay Kit (Abcam) (C). Expression of IFN- $\gamma$  and TNF- $\alpha$  in extracted infiltrating CD8<sup>+</sup> T cells tested by flow cytometry (D), and the summarized percentages of IFN- $\gamma$ <sup>+</sup> TNF- $\alpha$ <sup>+</sup> cells as proportions of CD3<sup>+</sup>CD8<sup>+</sup> T cells (E). (F–J) Transplanted subcutaneous MC38 EGFRvIII tumors from C57BL/6 mice were treated with CET+IRI, POM-1, CET+IRI+POM-1, CET+IRI+ $\alpha$ -PD-1 or CET+IRI+POM-1+ $\alpha$ -PD-1, respectively. In all regimens, the POM-1 dosing scheme comprised pretreatment of mice at a 5 mg/kg dose daily for 3 days, before initiation of combination treatment. Representative images of subcutaneous tumors from each group harvested on day 28 (F). Tumor growth curves on day 4–28 postinjection with MC38 EGFRvIII cells. Tumor volumes were calculated every 3 days ( $n=5$  per group) (G). P values were determined by two-way ANOVA. Expression of IFN- $\gamma$  and TNF- $\alpha$  in extracted infiltrating CD8<sup>+</sup> T cells analyzed by flow cytometry (H), and summarized percentages of IFN- $\gamma$ <sup>+</sup> TNF- $\alpha$ <sup>+</sup> cells as a proportion of CD3<sup>+</sup>CD8<sup>+</sup> T cells (I–J). (K–M) BALB/c mice carrying subcutaneous CT26 EGFRvIII tumors were treated with POM-1 or  $\alpha$ -PD-1, alone or in combination. Representative images of subcutaneous tumors from each group harvested on day 22 (K). Tumor growth curves on day 4–22 postinjection with CT26 EGFRvIII cells. Tumor volumes were calculated every 3 days ( $n=4$  per group) (L). P values were determined by two-way ANOVA. Expression of IFN- $\gamma$  and TNF- $\alpha$  in extracted infiltrating CD8<sup>+</sup> T cells determined by flow cytometry. Percentages of CD3<sup>+</sup>CD8<sup>+</sup> T cells (left panel) and IFN- $\gamma$ <sup>+</sup> TNF- $\alpha$ <sup>+</sup> cells (right panel) as proportions of CD3<sup>+</sup>CD8<sup>+</sup> T cells (M). Data are mean $\pm$ SEM values of at least three independent experiments. \* $P<0.05$ , \*\* $P<0.01$ , \*\*\* $P<0.001$ , and \*\*\*\* $P<0.0001$ . ADO, adenosine; ANOVA, analysis of variance; CI, cetuximab plus irinotecan; CRC, colorectal cancer; CET, cetuximab; EGFRvIII, EGFR variant type III; EGFRwt, wild-type EGFR; GZMB, granzyme B; IFN, interferon; IRI, irinotecan; ns, not significant; TME, tumor microenvironment; TNF- $\alpha$ , tumor necrosis factor alpha.

also explored the therapeutic implications of targeting ADO metabolism in both MC38 (MSI-H) and CT26 (MSS) syngeneic CRC models. Inhibiting CD39 boosted the efficacy of combination treatment of EGFRvIII MC38 (MSI-H) tumors with anti-PD-1 and CET. More importantly, inhibiting CD39 reversed anti-PD1 resistance in EGFRvIII CT26 (MSS) tumors, highlighting the potentially broad utility of an ADO-targeting approach in promoting immunotherapy efficacy in both MSI-H and MSS CRC tumors otherwise resistant to immune checkpoint blockade therapy. Notably, pretreatment with POM-1 achieved more significant therapeutic outcomes than conventional simultaneous administration. After 3 days of POM-1 administration, there was a notable improvement in CD8<sup>+</sup> T-cell infiltration in the TME, creating a suitable 'soil' for subsequent antitumor immune responses triggered by CET or ICIs. These results further emphasize the critical role of the immune microenvironment in anti-tumor therapy mechanisms and provide valuable insights to inform the design of combination strategies involving 'microenvironment modulators', such as POM-1, in conjunction with other tumor therapies.

As a constitutively active mutant of EGFR, EGFRvIII influences downstream pathways, including JAK/STAT signaling,<sup>20</sup> which is closely associated with migratory and invasive phenotypes mediated by EGFRvIII in glioblastoma.<sup>41</sup> EGFRvIII phosphorylation enhances downstream STAT signaling, and subsequent STAT3 phosphorylation depends on EGFRvIII nuclear translocation and interaction with STAT3 in the nucleus.<sup>41-42</sup> The EGFRvIII mutation also has a notable impact on the role of STAT3 in tumorigenesis; for example, STAT3 can inhibit the malignant transformation of astrocytes, while in the presence of EGFRvIII, STAT3 forms a complex with EGFRvIII in the nucleus, promoting tumorigenesis.<sup>20-43</sup> In this study, we observed a distinct elevation of p-STAT3 in nucleus of EGFRvIII cells. This finding underscores the close association between EGFRvIII and nuclear regulation of STAT3. Meanwhile, although the ADO pathway, mediated by CD39 and CD73, has emerged as a promising target for drug development, there is little research on the upstream mechanisms governing CD39 and CD73 regulation; notable regulators identified to date include hypoxia and TGFβ.<sup>30</sup> In our study, through gene set enrichment analysis, we found that CD39 and CD73 expression in EGFRvIII cells was associated with the STAT3 pathway. Moreover, our experiments using STAT3 inhibitors and siRNA validated that STAT3 positively regulates the expression of CD39 and CD73, providing further insights into ADO metabolism and expanding understanding of its regulation.

Identifying targets for improving immune infiltration through ADO metabolism and other pathways is currently the primary focus of research aiming to expand the applications of immunotherapy and develop combination immunotherapies. In CRC, the main obstacle to the efficacy of PD-1/PD-L1 checkpoint inhibitors is the 'cold tumor' phenotype, characterized by deficiency of

tumor neo-antigens and limited CD8<sup>+</sup> T-cell infiltration.<sup>2</sup> In our study, we observed promising therapeutic effects of POM-1 combination immunotherapy in EGFRvIII-mutant MSS CRC, resulting in an increased number of CD8<sup>+</sup> T cells and enhanced cytotoxicity within the tumor, indicating a transition from a 'cold' to a 'hot' tumor state. This study also has limitations. First, as the tissue sections were sourced exclusively from primary tumors, the expression of EGFRvIII and its effects on TME in metastatic lesions remain unassessed. Second, validating the regulation of ADO metabolism by EGFRvIII across larger and more diverse cell lines, animal models, and patient cohorts could strengthen these conclusions. Overall, our data highlight the potential of EGFRvIII as a novel biomarker for stratified diagnosis and treatment of MSS CRC.

#### Author affiliations

<sup>1</sup>Department of Oncology, Nanfang Hospital, Southern Medical University, Guangzhou, Guangdong, China

<sup>2</sup>Department of Experimental Radiation Oncology, The University of Texas MD Anderson Cancer Center, Houston, Texas, USA

<sup>3</sup>Department of Oncology, The First People's Hospital of Foshan, Foshan, Guangdong, China

<sup>4</sup>Department of Radiation Oncology, Zhujiang Hospital, Southern Medical University, Guangzhou, Guangdong, China

<sup>5</sup>Center of Gastrointestinal Surgery, The First Affiliated Hospital, Sun Yat-Sen University, Guangzhou, China

<sup>6</sup>Department of Oncology, Guangdong Provincial Hospital of Traditional Chinese Medicine, Guangzhou, China

X Xiaoxiang Rong @cancer

**Contributors** FS: conceptualization, methodology, validation, formal analysis, data curation, writing—original draft; FY: conceptualization, methodology, validation, writing—original draft; CZ: methodology, validation, formal analysis, data curation, visualization, writing—review and editing; YZ: conceptualization, formal analysis, data curation, writing—review and editing, visualization; BL: validation, investigation, data curation; SL: resources, methodology, data curation; YW: validation, investigation, data curation; QW: software, validation, investigation; YS: validation, investigation; ZY: validation, investigation; JW: investigation, methodology; YJ: software, investigation; CG: software, investigation; QH: methodology, validation; WL: conceptualization, resources, supervision, methodology; NH: resources, methodology; CW: resources, methodology; XR: resources, methodology; JW: resources, methodology; YT: resources, methodology; JP: resources, methodology; YL: resources, methodology; MS: conceptualization, resources, supervision, funding acquisition, validation, investigation, methodology, writing—review and editing. After unanimous agreement among all authors, the guarantor of this paper has been determined to be MS, the corresponding author. MS has been deeply involved in every aspect of the research process, from project approval and experimental supervision to the final review of the paper, overseeing all key steps. Familiar with the principles of scientific research integrity and journal publication standards, MS fully guarantees the authenticity of the data, the rationality and compliance of the research methods, and the absence of academic misconduct during the writing process. MS is also willing to bear full academic responsibility for any issues related to the paper.

**Funding** This work was supported by the National Natural Science Foundation of China (Grant number 82273271 to MS; Grant number 81803034 to YZ; Grant number 82103015 to QH), the Guangdong Basic and Applied Basic Research Foundation (Grant number 2022A1515011693 to MS), and the Beijing Bethune Charitable Foundation.

**Patient and public involvement statement** Patients and/or the public were not involved in the design, or conduct, or reporting, or dissemination plans of this research.

**Patient consent for publication** Not applicable.

**Ethics approval** All animal studies were conducted in accordance with guidelines approved by the Southern Medical University Animal Care and Use Committee (no. 44002100030936). The use of human tissue samples and clinical data was approved by the ethics committee of Nanfang Hospital (no. NFEC-2022-524). Informed consent was obtained from all participants or their legally authorized representatives included in the study.

**Provenance and peer review** Not commissioned; externally peer reviewed.

**Data availability statement** All data relevant to the study are included in the article or uploaded as supplementary information. Datasets generated and analyzed during this study are available from the corresponding author on reasonable request.

**Supplemental material** This content has been supplied by the author(s). It has not been vetted by BMJ Publishing Group Limited (BMJ) and may not have been peer-reviewed. Any opinions or recommendations discussed are solely those of the author(s) and are not endorsed by BMJ. BMJ disclaims all liability and responsibility arising from any reliance placed on the content. Where the content includes any translated material, BMJ does not warrant the accuracy and reliability of the translations (including but not limited to local regulations, clinical guidelines, terminology, drug names and drug dosages), and is not responsible for any error and/or omissions arising from translation and adaptation or otherwise.

**Open access** This is an open access article distributed in accordance with the Creative Commons Attribution Non Commercial (CC BY-NC 4.0) license, which permits others to distribute, remix, adapt, build upon this work non-commercially, and license their derivative works on different terms, provided the original work is properly cited, appropriate credit is given, any changes made indicated, and the use is non-commercial. See <http://creativecommons.org/licenses/by-nc/4.0/>.

#### ORCID iDs

Yu Jiang <http://orcid.org/0009-0009-2253-1033>

Wangjun Liao <http://orcid.org/0000-0002-1364-8442>

Min Shi <http://orcid.org/0000-0003-0113-4089>

#### REFERENCES

- 1 Le DT, Uram JN, Wang H, *et al.* PD-1 Blockade in Tumors with Mismatch-Repair Deficiency. *N Engl J Med* 2015;372:2509–20.
- 2 Akin Telli T, Bregni G, Vanhooren M, *et al.* Regorafenib in combination with immune checkpoint inhibitors for mismatch repair proficient (pMMR)/microsatellite stable (MSS) colorectal cancer. *Cancer Treat Rev* 2022;110:102460.
- 3 Chen L, Jiang X, Li Y, *et al.* How to overcome tumor resistance to anti-PD-1/PD-L1 therapy by immunotherapy modifying the tumor microenvironment in MSS CRC. *Clin Immunol* 2022;237:108962.
- 4 Misale S, Di Nicolantonio F, Sartore-Bianchi A, *et al.* Resistance to anti-EGFR therapy in colorectal cancer: from heterogeneity to convergent evolution. *Cancer Discov* 2014;4:1269–80.
- 5 Woolston A, Khan K, Spain G, *et al.* Genomic and Transcriptomic Determinants of Therapy Resistance and Immune Landscape Evolution during Anti-EGFR Treatment in Colorectal Cancer. *Cancer Cell* 2019;36:35–50.
- 6 Kawaguchi Y, Kono K, Mimura K, *et al.* Cetuximab induce antibody-dependent cellular cytotoxicity against EGFR-expressing esophageal squamous cell carcinoma. *Int J Cancer* 2007;120:781–7.
- 7 Srivastava RM, Lee SC, Andrade Filho PA, *et al.* Cetuximab-activated natural killer and dendritic cells collaborate to trigger tumor antigen-specific T-cell immunity in head and neck cancer patients. *Clin Cancer Res* 2013;19:1858–72.
- 8 Pozzi C, Cuomo A, Spadoni I, *et al.* The EGFR-specific antibody cetuximab combined with chemotherapy triggers immunogenic cell death. *Nat Med* 2016;22:624–31.
- 9 Stein A, Binder M, Goekkert E, *et al.* Avelumab and cetuximab in combination with FOLFOX in patients with previously untreated metastatic colorectal cancer (MCRC): Final results of the phase II AVETUX trial (AIO-KRK-0216). *JCO* 2020;38:96.
- 10 Tintinot J, Ristow I, Sauer M, *et al.* Translational analysis and final efficacy of the AVETUX trial - Avelumab, cetuximab and FOLFOX in metastatic colorectal cancer. *Front Oncol* 2022;12:993611.
- 11 Cen S, Liu K, Zheng Y, *et al.* BRAF Mutation as a Potential Therapeutic Target for Checkpoint Inhibitors: A Comprehensive Analysis of Immune Microenvironment in BRAF Mutated Colon Cancer. *Front Cell Dev Biol* 2021;9:705060.
- 12 Morris VK, Parseghian CM, Escano M, *et al.* Phase I/II trial of encorafenib, cetuximab, and nivolumab in patients with microsatellite stable, BRAF<sup>V600E</sup> metastatic colorectal cancer. *JCO* 2022;40:12.
- 13 Dong Z-Y, Zhang J-T, Liu S-Y, *et al.* EGFR mutation correlates with uninfamed phenotype and weak immunogenicity, causing impaired response to PD-1 blockade in non-small cell lung cancer. *Oncoimmunology* 2017;6:e1356145.
- 14 Song SG, Kim S, Koh J, *et al.* Comparative analysis of the tumor immune-microenvironment of primary and brain metastases of non-small-cell lung cancer reveals organ-specific and EGFR mutation-dependent unique immune landscape. *Cancer Immunol Immunother* 2021;70:2035–48.
- 15 Kumagai S, Koyama S, Nishikawa H. Antitumor immunity regulated by aberrant ERBB family signalling. *Nat Rev Cancer* 2021;21:181–97.
- 16 Wee P, Wang Z. Epidermal Growth Factor Receptor Cell Proliferation Signaling Pathways. *Cancers (Base)* 2017;9:52.
- 17 Eskilsson E, Rosland GV, Talasila KM, *et al.* EGFRVIII mutations can emerge as late and heterogenous events in glioblastoma development and promote angiogenesis through Src activation. *Neuro Oncol* 2016;18:1644–55.
- 18 Sok JC, Coppelli FM, Thomas SM, *et al.* Mutant epidermal growth factor receptor (EGFRVIII) contributes to head and neck cancer growth and resistance to EGFR targeting. *Clin Cancer Res* 2006;12:5064–73.
- 19 Wheeler SE, Suzuki S, Thomas SM, *et al.* Epidermal growth factor receptor variant III mediates head and neck cancer cell invasion via STAT3 activation. *Oncogene* 2010;29:5135–45.
- 20 An Z, Aksoy O, Zheng T, *et al.* Epidermal growth factor receptor and EGFRVIII in glioblastoma: signaling pathways and targeted therapies. *Oncogene* 2018;37:1561–75.
- 21 Jutten B, Dubois L, Li Y, *et al.* Binding of cetuximab to the EGFRVIII deletion mutant and its biological consequences in malignant glioma cells. *Radiother Oncol* 2009;92:393–8.
- 22 An Z, Knobbe-Thomsen CB, Wan X, *et al.* EGFR Cooperates with EGFRVIII to Recruit Macrophages in Glioblastoma. *Cancer Res* 2018;78:6785–94.
- 23 Khelwatty SA, Essapen S, Bagwan I, *et al.* Co-expression and prognostic significance of putative CSC markers CD44, CD133, wild-type EGFR and EGFRVIII in metastatic colorectal cancer. *Oncotarget* 2019;10:1704–15.
- 24 Cunningham MP, Essapen S, Thomas H, *et al.* Coexpression, prognostic significance and predictive value of EGFR, EGFRVIII and phosphorylated EGFR in colorectal cancer. *Int J Oncol* 2005;27:317–25.
- 25 Khelwatty S, Essapen S, Bagwan I, *et al.* The impact of co-expression of wild-type EGFR and its ligands determined by immunohistochemistry for response to treatment with cetuximab in patients with metastatic colorectal cancer. *Oncotarget* 2017;8:7666–77.
- 26 Azuma M, Danenberg KD, Iqbal S, *et al.* Epidermal growth factor receptor and epidermal growth factor receptor variant III gene expression in metastatic colorectal cancer. *Clin Colorectal Cancer* 2006;6:214–8.
- 27 Xiao Y, Ma D, Zhao S, *et al.* Multi-Omics Profiling Reveals Distinct Microenvironment Characterization and Suggests Immune Escape Mechanisms of Triple-Negative Breast Cancer. *Clin Cancer Res* 2019;25:5002–14.
- 28 Ayers M, Lunceford J, Nebozhyn M, *et al.* IFN- $\gamma$ -related mRNA profile predicts clinical response to PD-1 blockade. *J Clin Invest* 2017;127:2930–40.
- 29 Vijayan D, Young A, Teng MWL, *et al.* Targeting immunosuppressive adenosine in cancer. *Nat Rev Cancer* 2017;17:709–24.
- 30 Allard B, Allard D, Buisset L, *et al.* The adenosine pathway in immuno-oncology. *Nat Rev Clin Oncol* 2020;17:611–29.
- 31 Wu J, Liu W, Williams JP, *et al.* EGFR-Stat3 signalling in nerve glial cells modifies neurofibroma initiation. *Oncogene* 2017;36:1669–77.
- 32 Liu Z, Ma L, Sun Y, *et al.* Targeting STAT3 signaling overcomes gefitinib resistance in non-small cell lung cancer. *Cell Death Dis* 2021;12:5611.
- 33 Song H, Wang R, Wang S, *et al.* A low-molecular-weight compound discovered through virtual database screening inhibits Stat3 function in breast cancer cells. *Proc Natl Acad Sci USA* 2005;102:4700–5.
- 34 Shuai C, Xia GQ, Yuan F, *et al.* CD39-mediated ATP-adenosine signalling promotes hepatic stellate cell activation and alcoholic liver disease. *Eur J Pharmacol* 2021;905:174198.
- 35 Yang R, Elsaadi S, Misund K, *et al.* Conversion of ATP to adenosine by CD39 and CD73 in multiple myeloma can be successfully targeted together with adenosine receptor A2A blockade. *J Immunother Cancer* 2020;8:e000610.
- 36 Zhou J, Ji Q, Li Q. Resistance to anti-EGFR therapies in metastatic colorectal cancer: underlying mechanisms and reversal strategies. *J Exp Clin Cancer Res* 2021;40:328.

- 37 Li Q-H, Wang Y-Z, Tu J, *et al.* Anti-EGFR therapy in metastatic colorectal cancer: mechanisms and potential regimens of drug resistance. *Gastroenterol Rep (Oxf)* 2020;8:179–91.
- 38 Van Den Eynde M, Huyghe N, De Cuyper A, *et al.* Interim analysis of the AVETUXIRI Trial: Avelumab combined with cetuximab and irinotecan for treatment of refractory microsatellite stable (MSS) metastatic colorectal cancer (mCRC)—A proof of concept, open-label, nonrandomized phase IIa study. *JCO* 2021;39:80.
- 39 Passarelli A, Aieta M, Sgambato A, *et al.* Targeting Immunometabolism Mediated by CD73 Pathway in *EGFR*-Mutated Non-small Cell Lung Cancer: A New Hope for Overcoming Immune Resistance. *Front Immunol* 2020;11:1479.
- 40 Moesta AK, Li XY, Smyth MJ. Targeting CD39 in cancer. *Nat Rev Immunol* 2020;20:739–55.
- 41 Zhang M, Sun H, Deng Y, *et al.* COPI-Mediated Nuclear Translocation of EGFRvIII Promotes STAT3 Phosphorylation and PKM2 Nuclear Localization. *Int J Biol Sci* 2019;15:114–26.
- 42 Fan QW, Cheng CK, Gustafson WC, *et al.* EGFR phosphorylates tumor-derived EGFRvIII driving STAT3/5 and progression in glioblastoma. *Cancer Cell* 2013;24:438–49.
- 43 de la Iglesia N, Konopka G, Puram SV, *et al.* Identification of a PTEN-regulated STAT3 brain tumor suppressor pathway. *Genes Dev* 2008;22:449–62.